v_2 vs p_T in p+Au at RHIC

by

Theodore Koblesky

B.S., University of Illinois, 2011

A thesis submitted to the

Faculty of the Graduate School of the

University of Colorado in partial fulfillment

of the requirements for the degree of

Doctor of Philosophy

Department of Physics

2017

This thesis entitled:
v_2 vs p_T in p+Au at RHIC
written by Theodore Koblesky
has been approved for the Department of Physics

_____

Prof. James Nagle

_____

Prof. Standin

_____

Ms. Standin

Date _____

The final copy of this thesis has been examined by the signatories, and we find that both the content and the form meet acceptable presentation standards of scholarly work in the above mentioned discipline.

Koblesky, Theodore (Ph.D., High Energy Nuclear Physics)

v_2 vs p_T in p+Au at RHIC

Thesis directed by Prof. James Nagle

Abstract

Here is a default abstract. Here is a default abstract. Here is a default abstract. Here is a default abstract. Here is a default abstract. Here is a default abstract. Here is a default abstract. Here is a default abstract. Here is a default abstract. Here is a default abstract. Here is a default abstract. Here is a default abstract. Here is a default abstract. Here is a default abstract. Here is a default abstract. Here is a default abstract. Here is a default abstract. Here is a default abstract. Here is a default abstract.

Dedication

To some of the of the fluffy kitties.

Acknowledgements

People

Contents

Tables

Table

Figures

Figure

Chapter 1

Collectivity and Flow in QCD Systems

1.1 A Conceptual Understanding of Collectivity and Flow

The observation of collectivity in matter can be a powerful indicator of fundamental properties in that matter. Collectivity means many discrete structures are interacting together to form a whole otherwise known as highly correlated behavior. In high energy heavy ion physics, a common interpretation of this behavior, although not the only interpretation[1] , is of a locally equilibrated medium with bulk properties instead of a group of individually interacting constituent particles. In this case, the medium would be QGP and the bulk properties would be that of a hydrodynamically described fluid: viscosity, density, temperature, etc. The term collectivity is often synonymous with the term hydrodynamic flow or simply flow. In this thesis, the terms will be used synonymously except in specific cases where the distinction is important.

It is important to note that although collectivity has a distinct signal, there are possible sources that can produce such a signal which do not involve collective behavior. These sources are called "non-flow" to differentiate them from sources of collectivity, such as flow. Especially true in small collision systems, non-flow is the largest background component when measuring collectivity. Thus, when making measurements, often non-flow must be taken into account as either a systematic uncertainty or as a systematic error correction. Sources of non-flow will be discussed more in Chapter 5 section .xxx.

[1] Although it is common to think of collectivity as hydrodynamic behavior, observations of collectivity do not necessarily imply any specific interpretation. Later we will discuss some alternative interpretations such as glasma correlations.

To assist in the discussion of flow, we will describe how it is measured briefly. Generally flow can be observed in heavy ion collisions by looking for long-range angular correlations in the spray of final state particles that come out of the collision. "Long-range angular correlations" in this case refers to correlations in particles with trajectories that have a large separation in pseudorapiditiy η. When looking for correlations, this separation in η ensures that we are measuring something other than just local correlations, which are often due to non-flow.

Conceptually, the story of flow is that patterns in the initial conditions of the medium will be carried through the medium evolution and observable in the final state particles. Figure 1.1 demonstrates the key events in the story: initial state geometry becomes transformed into a final state momentum anisotropy. The consideration of initial collision geometry will be a reoccurring theme when interpreting results in this thesis because the initial state geometry is one of the few independent variables over which we have experimental control.

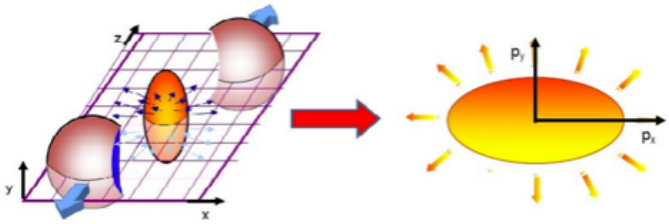

Figure 1.1: A diagram demonstrating the relation between initial state geometry being transformed into final state momentum anisotropy. The left depicts two spherical nuclei colliding parallel to the z-axis. The pair of nuclei leave behind ellipsoid corresponding to the almond-shaped elliptical overlap region present in the initial state collision geometry. This ellipsoid hydrodynamically evolves such that it expands along the steepest pressure gradient which corresponds to the transverse (x-y plane). The right depicts the elliptical pattern present in transverse momentum distribution of the final state particles after the medium has finished evolving.

1.1.1 Initial Conditions

Before proceeding in describing flow mathematically, it is useful to talk about the initial conditions of heavy ion collisions.

$$\epsilon_n = \frac{\sqrt{< r^2 \cos(n\phi) >^2 + < r^2 \sin(n\phi) >^2}}{< r^2 >}, \tag{1.1}$$

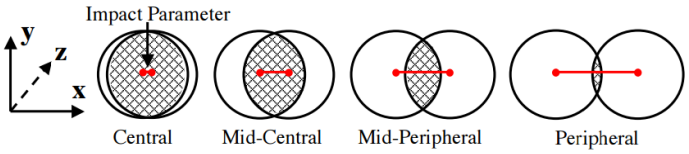

Figure 1.2: A diagram demonstrating the relation between initial state geometry being transformed into final state momentum anisotropy. The left depicts two spherical nuclei colliding parallel to the z-axis. The pair of nuclei leave behind ellipsoid corresponding to the almond-shaped elliptical overlap region present in the initial state collision geometry. This ellipsoid hydrodynamically evolves such that it expands along the steepest pressure gradient which corresponds to the transverse (x-y plane). The right depicts the elliptical pattern present in transverse momentum distribution of the final state particles after the medium has finished evolving.

1.2 Mathematical Introduction to Measuring and Quantifying Flow

As discussed above, looking for long-range angular correlations is a way to measure flow. Measuring the azimuthal anisotropy is a way to quantify the extent of long-range angular correlation present in the medium evolution. Azimuthal anisotropy is the degree to which measured particles are non-uniform in the transverse plane. There are a number of ways to measure the azimuthal anisotropy. We will start by creating a correlation function.

1.2.1 Two-Particle Correlations

A correlation function is dependent on the difference in particles' trajectories, rather than the trajectories of the particles themselves. Let us consider the two-particle correlation function which uses **pairs** of particles from a collision event in order to create a correlation function. For

each each pair in an event, a $\Delta\phi = \phi_1$ - ϕ_2, and a $\Delta\eta = \eta_1$ - η_2, value is obtained which makes up the signal $S(\Delta\phi, \Delta\eta)$ for a single event:

$$S(\Delta\phi, \Delta\eta) = \sum_{j=1}^{N_{\text{particles}}} \left(\sum_{i=j+1}^{N_{\text{particles}}} s(\phi_i - \phi_j, \eta_i - \eta_j) \right) = \sum_{k=1}^{N_{\text{pairs}}} s(\Delta\phi_k, \Delta\eta_k), \tag{1.2}$$

where $s(\phi_i - \phi_j, \eta_i - \eta_j) = s(\Delta\phi_k, \Delta\eta_k)$ is a single pair in an event, $N_{\text{particles}}$ is the number of particles in an event, and N_{pairs} is the number of unique pairs in an event. This pair counting scheme ensures that no pair will be double counted and that a particle can not form a pair with itself.

Ideally, this $S(\Delta\phi, \Delta\eta)$ would be the correlation function; however, there are artificial correlations due to detector acceptance and other sources which would distort this distribution. In order to correct for these effects, a mixed event background distribution $M(\Delta\phi, \Delta\eta)$ is created, whereby pairs are produced by particles from two different events. Then correlation function can be defined as follows:

$$C(\Delta\phi, \Delta\eta) = \frac{S(\Delta\phi, \Delta\eta)}{M(\Delta\phi, \Delta\eta)} \frac{\int M(\Delta\phi, \Delta\eta)\, d\Delta\phi d\Delta\eta}{\int S(\Delta\phi, \Delta\eta)\, d\Delta\phi d\Delta\eta}, \tag{1.3}$$

where the integration is over the full $\Delta\phi, \Delta\eta$ range in order to normalize the correlation function. Substantial variations in this $C(\Delta\phi, p_T)$ are usually seen as long-range angular correlations which can be attributed to collectivity.

In practice, correlation functions often combine particles from two variable p_T ranges. The first p_T range is known as the "trigger particles" and the second range is known as the "associated" particles. In this scheme, the pair function is $s(\phi_i^t - \phi_j^a, \eta_i^t - \eta_j^a)$ where the t superscript indicates trigger particles with a given p_T range and the a superscript indicates associated particles with a given p_T range.

An example of two 2-D two-particle correlation functions for $p + p$ at $\sqrt{s_{NN}}$= 7 TeV with no multiplicity selection $Pb + Pb$ at $\sqrt{s_{NN}}$= 2.76 TeV high multiplicity events is shown in Figure 1.3. The trigger and associated p_T ranges are given in the figure caption. Plotting the correlation

function in terms of both $\Delta\phi$ and $\Delta\eta$ allows one to see the full extent and location of correlations for the collision system. These two correlations were selected to showcase the two extremes of typical correlation functions.

An important feature in the left plot shows a large amount of correlations at $(\Delta\phi, \Delta\eta) =$ (0,0), which is known as the nearside[2] "jet peak." As mentioned in Chapter 1, jets are a spray of particle in a cone shape; therefore, the jet peak is at (0,0) because all the particles within the jet have nearly the same trajectory. The jet peak has been truncated for plotting reasons because it is so large. Another important feature is what is known as the "awayside ridge" or "awayside jet peak" located at π and extending very far in the $\Delta\eta$ variable. This feature arises when back-to-back dijets are produced; all of the particles from one of the jets will be roughly π radians apart in trajectory with respect to the other jet and spread out in $\Delta\eta$. Apart from these main features which come from jets and dijets, there are no other sources of systematic correlations between particles for minimum bias $p+p$ events, such that $p+p$ events are taken to be the representation of the non-flow background. Thus, correlation function features present in regular $p+p$ events are taken to be present at some level in the correlation function of every heavy ion collision system.

Conversely, the right panel of 1.3 depicts the correlation function of high multiplicity $Pb+Pb$ events which exhibit characteristics of flow. While the non-flow features of the nearside jet peak and the awayside peak are present, a new feature known as the "nearside ridge" is located at $(\Delta\phi, \Delta\eta) = (0, |\Delta\eta| >\sim 1.0)$. This ridge exists in contrast to the lack of any correlations in the $p+p$ correlation function at that location. It should be noted that the awayside jet ridge has also been modified by the bulk of particles. The nearside ridge and the awayside ridge modification are due to particles with long-range angular correlations. Thus, by quantifying the magnitude of these effects, the degree to which flow is present in the system can be measured.

[2] For correlation functions, $\Delta\phi \sim 0$ is known as "nearside" and $\Delta\phi \sim \pi$ is known as "awayside."

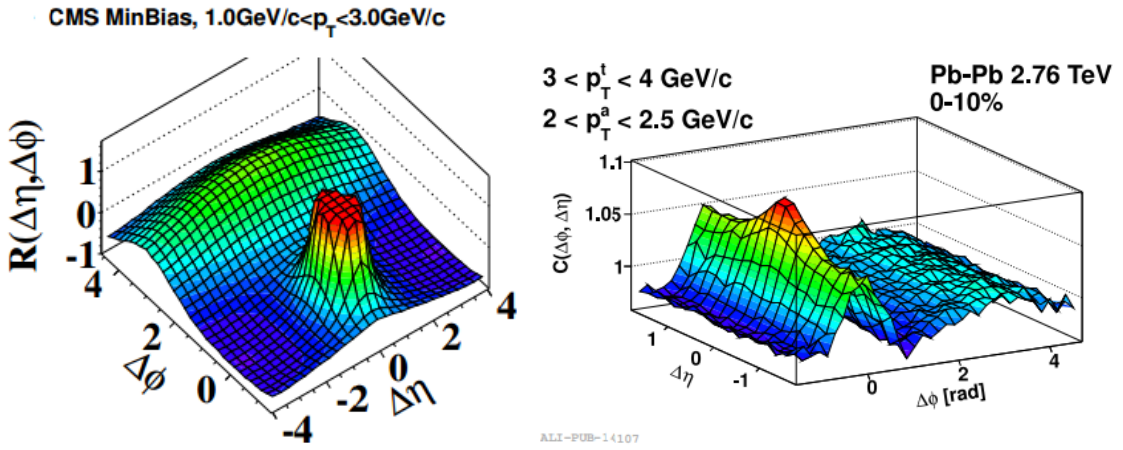

Figure 1.3: The right plot is 2-D two-particle correlation function for $p+p$ collisions at $\sqrt{s_{NN}}$= 7 TeV for hadrons with the same trigger and associated p_T range of $1.0 < |p_T| < 3.0$ GeV/c for all events [19]. The left plot is 2-D two-particle correlation function for $Pb+Pb$ collisions at $\sqrt{s_{NN}}$= 2.76 TeV 0-10%centrality events for trigger hadrons with $3 < p_T^t < 4$ GeV/c and associated hadrons with $2 < p_T^t < 2.5$ GeV/c measured by ALICE. **add ref**.

1.2.2 Flow Harmonics

At this point, it useful to narrow our focus to the region of the correlation function which has long-range angular correlations by taking a projection in $\Delta\phi$ away from the jet peak at $\Delta\eta = 0$. This 1-D two-particle correlation function slice contains the azimuthal anisotropy which should correspond to the degree of flow present in the system. Figure 1.4 depicts this correlation function $C(\Delta\phi)$ for central $Pb+Pb$ events. In order to quantify the azimuthal anisotropy, $C(\Delta\phi)$ is cos Fourier expanded:

$$C(\Delta\phi) \propto 1 + \sum_{n=1} 2v_n \cos(n[\Delta\phi]), \tag{1.4}$$

where v_n are known as flow coefficients or flow harmonics and n is the harmonic order. The colored curves in Figure 1.4 are the first five components of the Fourier decomposition and their amplitudes show their relative strength. The green curve, which peaks at $\Delta\phi = 0$ and π, corresponds to the second order harmonic, which is related to the second order flow coefficient v_2. The reason v_2 is singled out is because it corresponds to elliptic flow and because it is the observable measured in

this thesis. In order to extract v_2 from this, one must calculate c_2 defined as:

$$c_2^{t,a} = \left\langle \cos(2(\phi_1^t - \phi_2^a) \right\rangle, \tag{1.5}$$

where $\langle\rangle$ is defined as the average over each event and all events and where ϕ_1^t and ϕ_1^a is the trigger and associated particles' ϕ, respectively. If the trigger and associated particles sets are the same then $\sqrt{c_2} = v_2$; however, if the trigger and associated particle sets are not the same then $c_2^{t,a}$=$v_2^t \times v_2^a$, wherev_2^t is the v_2 for the set of trigger particles alone and the same with v_2^a. This ability to resolve c_2 into the two distinct v_2 components is only true if factorization holds, which only occurs when the non-flow component of the measurement is small enough.

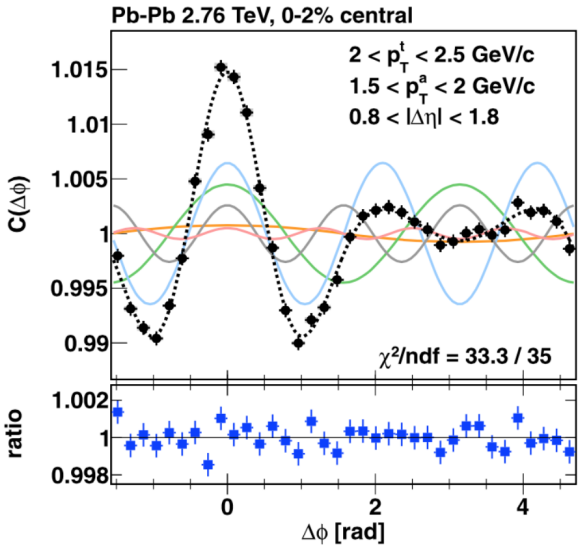

Figure 1.4: The 1-D correlation function in $Pb + Pb$ at $\sqrt{s_{NN}}$= 2.76 TeV for the most central events for for trigger hadrons with $2 < p_T^t < 2.5$ GeV/c and associated hadrons with $1.5 < p_T^t < 2$ GeV/c. The 1-D two-particle correlation function is a projection in $0.8 < |\Delta\eta| < 1.8$ from the 2-D correlation function, the 2-D correlation function being similar to that of the right panel of Figure 1.3. The black dotted points are the values of the correlation function and the colored lines are the first five cos Fourier decomposition components. The black dotted line is the sum of these five components. **add ref**.

1.2.3 Cumulants

Although two-particle correlations are useful, four-particle correlations or more can be used to better understand the flow measurement. In a multi-particle cumulant treatment, $c_n\{k\}$ measures the nth harmonic from groups of k particles while explicitly subtracting correlations from $< k$ particles. In this formulation, two-particle cumulants are treated the same way as in two-particle correlation functions:

$$v_2\{2\} = \sqrt{c_2\{2\}} = \sqrt{\langle \cos(2(\phi_1 - \phi_2))\rangle}, \tag{1.6}$$

whereas four-particle cumulants are defined as:

$$v_2\{4\} = (-c_2\{4\})^{1/4} = (2\langle \cos(2(\phi_1 - \phi_2))\rangle)^2 - \langle \cos(2(\phi_1 + \phi_2 - \phi_3 - \phi_4))\rangle)^{1/4}, \tag{1.7}$$

where the term with four ϕ indices corresponds to the four-particle correlation and the term with two ϕ indices corresponds to the subtracted off two-particle correlation term. Multi-particle cumulants are well defined for larger groupings of particles, $v_2\{6\}$, $v_2\{8\}$, and up. Comparing v_2 measured by two and four-particle cumulants is useful when estimating the level of fluctuations present in the system, something which will be discussed more in Section .xxx.

1.2.4 Event Plane Formulation

Another mathematical treatment for determining flow coefficients involves measuring a mathematical object known as an "event plane." Conceptually, the event plane method is an attempt to measure the reaction plane angle, which defines the plane to which it is aligned with the orientation of the initial state collision geometry. Figure 1.5 is a geometric diagram defining the reaction plane angle Ψ_{RP}.

The event plane method uses final state particles to calculate the event plane angle from the data. A different event plane angle is defined for each harmonic, and is denoted as Ψ_n where n is the harmonic number. For an event with N particles, define the flow vector $\vec{Q}$ as follows:

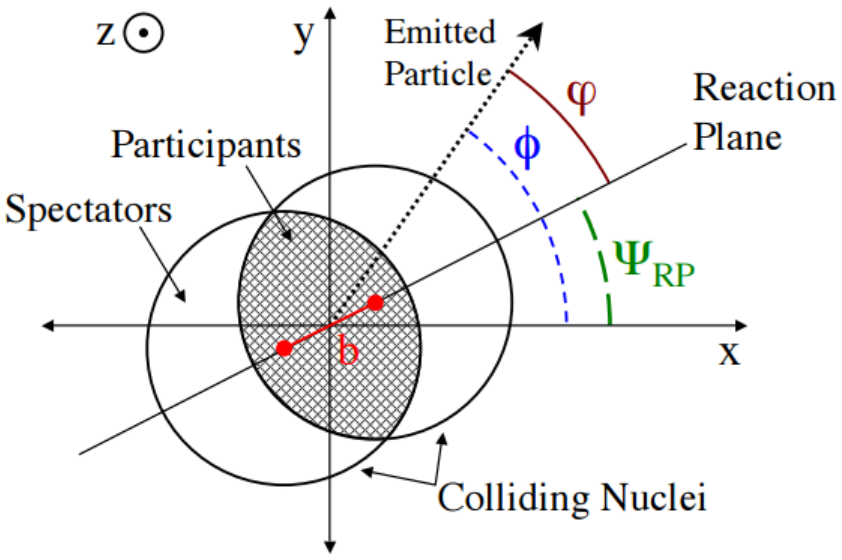

Figure 1.5: Diagram showing from the beams point of view several variables used to characterize events. The spectators are the nucleons which do not participate in the collision, as opposed to the participants which do participate in the collision. The impact parameter denoted as b and Ψ_{RP} is the reaction or participant plane angle. ϕ is the standard azimuthal and $\varphi = \phi$ - Ψ_{RP}. **add ref**

$$Q_x = \sum_i^N (w_i * \cos(n * \phi_i)) \tag{1.8}$$

$$Q_y = \sum_i^N (w_i * \sin(n * \phi_i)) \tag{1.9}$$

$$Q_w = \sum_i^N (w_i) \tag{1.10}$$

where i is the ith particle in the event, ϕ_i is the azimuthal angle of the particle, w_i is the weight factor, and n is the harmonic number.

We define the nth order event plane as

$$\Psi_n = \arctan\left(\frac{Q_y}{Q_x}\right)$$

Once the event plane has been calculated, the flow harmonics (v_n) are defined as

$$v_n = \frac{\langle\langle \cos(n(\phi - \Psi_n))\rangle\rangle}{Resolution(\Psi_n)}, \tag{1.11}$$

where $\langle\langle\rangle\rangle$ indicates that $\cos(2\phi - \psi)$ is averaged over all particles in the same event, and the resulting v_2 must be averaged over many events [24].

The event plane resolution is calculated using the standard 3-sub event method[24]. The strategy of this method is to measure Ψ_n with three different detectors in the same event, in order to better constrain the overall measurement of Ψ_n. The event plane resolution is defined as

$$Res(\Psi_n^A) = \sqrt{\frac{\langle\cos(n(\Psi_n^A - \Psi_n^B))\rangle \langle\cos(n(\Psi_n^A - \Psi_n^C))\rangle}{\langle\cos(n(\Psi_n^B - \Psi_n^C))\rangle}}, \tag{1.12}$$

where A,B, and C are three detectors measuring the same event. In this context, the term "sub-event" refers to the specific subset of particles measured by a given detector, assuming no decorrelation [24].

1.3 A Review of Flow Measurements in Small Collision Systems

As noted at the end of Chapter 1, small collision systems have been considered too small to create hot and dense matter. These systems were utilized as control experiments which measure how the presence of a nucleus would effect the production of particles relative to $p + p$ collisions. These so called "cold nuclear matter" (CNM) effects were isolated when colliding very low Z nuclei, such as a deuteron or proton, with a large nucleus.[3] Generally accepted CNM effects are: nuclear shadowing, which is the modification of parton distribution functions by a nucleus; gluon saturation, radiative energy loss which is the modification of the momentum fraction of partons due to multiple soft scatterings; and finally the Cronin effect, which is the broadening of the transverse momentum of emitted particles distribution due to multiple scatterings of initially colliding partons. **add ref**

1.3.1 Nearside Ridge in Small Systems

In 2010, the CMS collaboration published a paper observing a nearside ridge in high multiplicity 7 TeV $p + p$ events in the two-particle correlation function for dihadrons as shown in the left Figure 1.6. The aforementioned nearside ridge is located at $\Delta\phi = 0$ and at $|\Delta\eta| > 2$ in the

[3] A side note: the convention in the field of heavy ion physics is to label any such small system collisions as p+A and any large system collisions as A+A

figure. The ridge is significant in contrast to the $p+p$ correlation function shown in the right panel of Figure 1.6 with an absence of any such ridge.

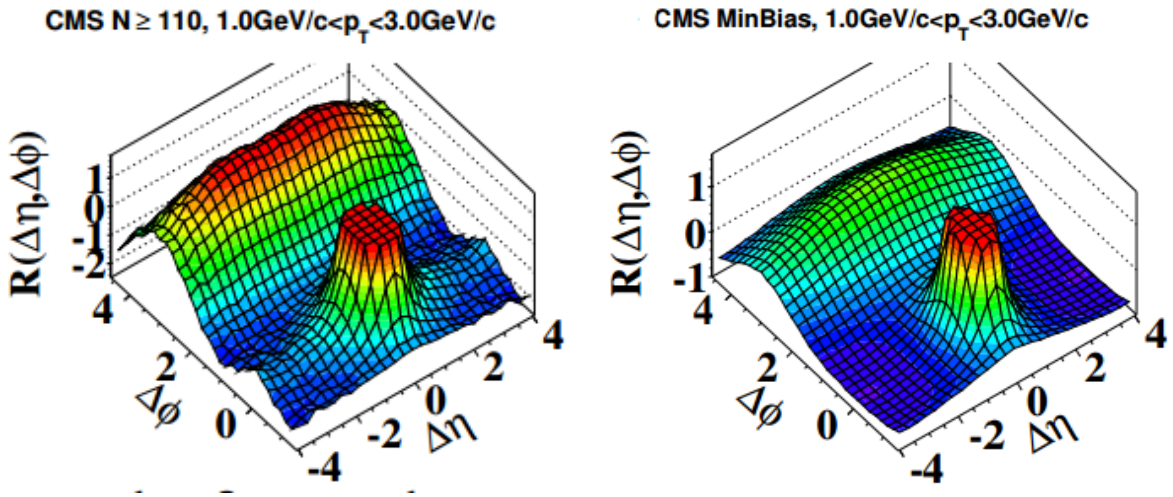

Figure 1.6: 2-D two-particle correlation function for $p+p$ collisions at $\sqrt{s_{NN}}$= 7 TeV for hadrons with $1.0 < |p_T| < 3.0$ GeV/c in high multiplicity events, with greater than 109 charged particles, and for any multiplicity of events are shown in the left and right panels, respectively[19].

What this discovery showed was that collectivity-like effects could be measured in small collisions systems for high-multiplicity events. Thus, $p + Pb$ at $\sqrt{s_{NN}}$= 5.02 TeV events were also analyzed to find flow and a nearside ridge was observed in 0-20% central events. It became apparent over the course of making these measurements that the non-flow contribution to the signal would be much larger for p+A events then that of A+A events. A procedure to reduce the non-flow component in the flow measurement is demonstrated in Figure 1.7. The procedure measures the same two-particle correlation function for central and peripheral events, in this case 0-20% central and 60-100% central and then subtracts the central correlation function by the peripheral one. The assumption is that the level and shape of the non-flow is mostly consistent across centrality classes, whereas the flow is centrality dependent, such that there is virtually no flow in the peripheral correlation function. Thus, by subtracting the central correlation function by the peripheral, only the like components to both will be subtracted out, which are the non-flow components. As seen in panel three in Figure 1.7, the subtracted correlation function has no dominating jet peak at (0,0)

and the nearside and awayside ridges are distinct and clear.

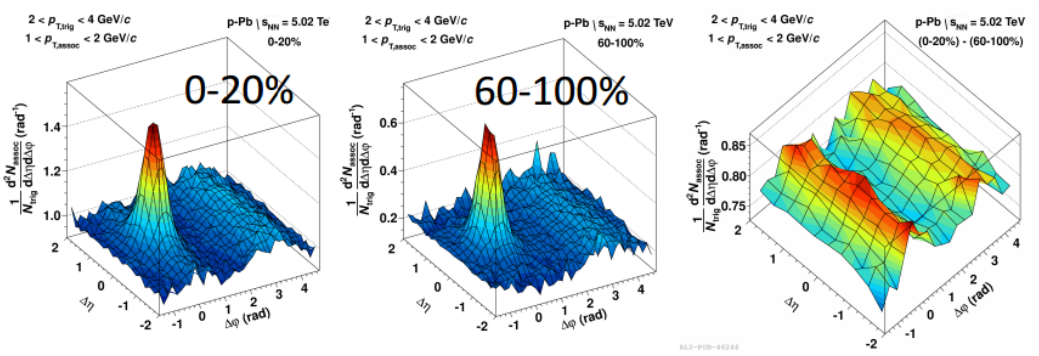

Figure 1.7: 2-D two-particle dihadron correlation function for $p + Pb$ collisions for 0-20% and 60-100% centrality events as measured by the ALICE detector in the left and middle panel, respectively. The rightmost panel shows the subtraction of the left panel by the middle panel to remove background. [?]

1.3.2 Mass Ordering in v_2

A key observation in the determination of real collective flow is a mass ordering in the strength of the flow coefficients. The left panel of Figure 1.8 depicts the observed mass ordering of particles in $Pb + Pb$ 10-20% centrality events. In the low p_T region of 0 - 2 GeV, there is an ordering in the magnitude of v_2 for hadrons: $\pi^{\pm} > K^{\pm} > p + pbar$ and so on for other heavier particles. This order is the opposite in which the hadrons are ordered by mass. The $\pi^{\pm}$ v_2 is the largest while the $\pi^{\pm}$ mass is the smallest. The mass ordering effect can be thought of as primarily a reduction in the v_2 for low p_T heavy hadrons. Assuming an elliptic flow is present, the steep pressure gradients will efficiently modify the magnitude of p_T for heavy hadrons more than for light hadrons, leading to a reduction in the number of heavy hadrons available at low p_T to produce a low p_T v_2 [17]. Thus, the mass ordering observation is taken to be evidence that the system is creating a medium such that particles will flow in predictable ways.

The right panel of Figure 1.8 shows a similar plot to the left panel of that figure except for the system $p + Pb$ $\sqrt{s_{NN}}$= 5.02 TeV. As in the $Pb + Pb$ system, the $p + Pb$ dataset exhibits a the

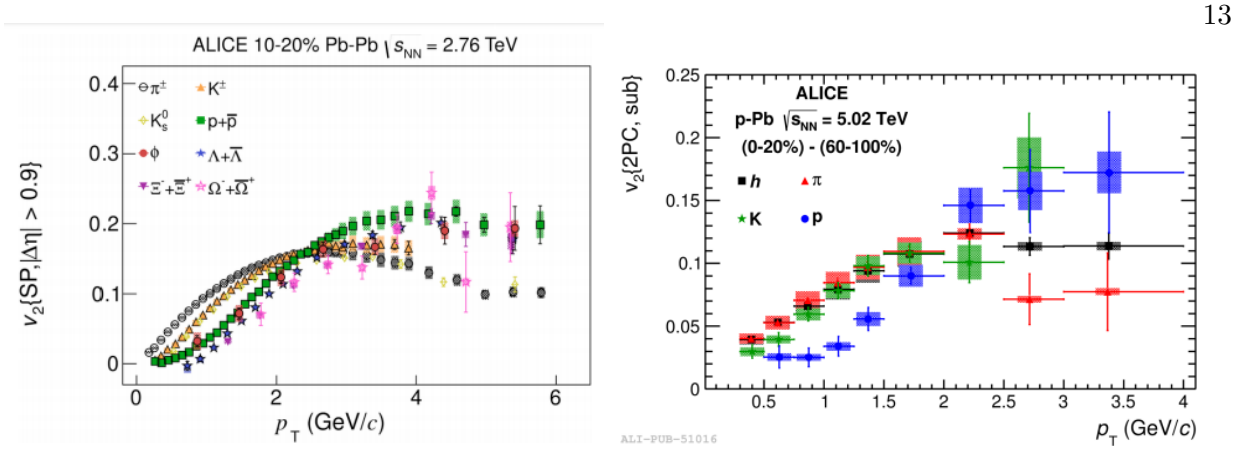

Figure 1.8: $v_2(p_T)$ for different particles (see legend) in Pb-Pb $\sqrt{s_{NN}}$= 2.76 TeV 10-20% events as measured by the ALICE detector. The $\Delta\eta$ gap at minimum is 0.9 units. The right plot shows the $v_2(p_T)$ for different particles (see legend) in p-Pb $\sqrt{s_{NN}}$= 5.02 TeV for 0-20% events that were subtracted by peripheral 60-100% events. The v_2 is extracted directly from the two particle correlation function shown in Figure 1.7. **add refs**

same mass ordering, as well as similar shapes of each $v_2(p_T)$ curve. Thus, the mass ordering effect that is observed in AA is also observed is small systems, such as pA. An important note for the result on the right panel is that a central minus peripheral subtraction was done, as demonstrated in Figure 1.7, whereas the result in the left panel needed no such peripheral subtraction. This means it is difficult to compare directly with the A+A result in magnitude, although the similarity of the ordering and the shape of the curves is enough of a comparison to indicate collectivity in the small system.

1.3.3 Multi-Particle Cumulants and Fluctuations

The effects of fluctuations in the elliptic flow measurement have been studied in small systems. In this context, fluctuations are effects which produce systematic correlations between particles from sources other than flow. Fluctuations can be thought of as correlations of a few particles in many events, rather than flow which is the correlations of many particles in a single event. Fluctuations are related to non-flow but are not identical. Fluctuations in the initial eccentricity can arise from fluctuations in the impact parameter within a centrality class of events and from fluctuations of

the initial positions of the participant nucleons [1].

In order to better understand the effect of fluctuations in our small systems measurements, v_2 was measured in different ways such as, $v_2\{2\}$ and $v_2\{4\}$, which are given by equations 1.5 and 1.6, respectively. The quantity $v_2\{2\}$ is the same as the two-particle correlation v_2, shown in Figure 1.8, while the quantity $v_2\{4\}$ is a four-particle correlation. This paper referenced here [1], defines a fluctuation term similar in form to standard deviation that is related to flow coefficients defined:

$$\sigma_\nu^2 \equiv \left\langle \nu^2 \right\rangle - \left\langle \nu \right\rangle^2, \tag{1.13}$$

where ν is the flow coefficient relative to the participant plane. This fluctuation term is related to $v_2\{2\}$ and $v_2\{4\}$ as

$$\nu\{2\}^2 = \left\langle \nu^2 \right\rangle = \left\langle \nu \right\rangle^2 + \sigma_\nu^2, \tag{1.14}$$

and

$$\nu\{4\}^2 = (2\left\langle \nu^2 \right\rangle^2 - \left\langle \nu^4 \right\rangle)^{1/2} \approx \left\langle \nu \right\rangle^2 - \sigma_\nu^2. \tag{1.15}$$

Thus, $v_2\{2\}$ measures the true elliptical flow plus fluctuations, whereas $v_2\{4\}$ measures the true elliptical flow minus fluctuations. By measuring both $v_2\{2\}$ and $v_2\{4\}$ for the same dataset, an estimate of the size of the fluctuations can be obtained. The difference between the two and four particle cumulants should be $\approx$ twice the size of the fluctuations.

Figure 1.9 shows the measurement of multi-particle cumulants in $p+p$, $p+Pb$, and $Pb+Pb$ by the CMS collaboration at the LHC. A key part of this plot is noticing the significant difference between $v_2\{2\}$ and $v_2\{4\}$ in high multiplicity $p+Pb$ and $Pb+Pb$ events, indicating the presence of fluctuations. In the $p+Pb$ and $Pb+Pb$ there is an apparent multiplicity threshold, approximately around $N_{trk}^{offline} = 75$, below which a class of peripheral events have a different kind of behavior than the high multiplicity events.

It is also interesting to note that for both systems, the $v_2\{4\}$, $v_2\{6\}$, $v_2\{8\}$, $v_2\{LYZ\}$ are in excellent agreement. The $v_2\{LYZ\}$ is v_2 measured taking into account the Lee-Yang zeros by

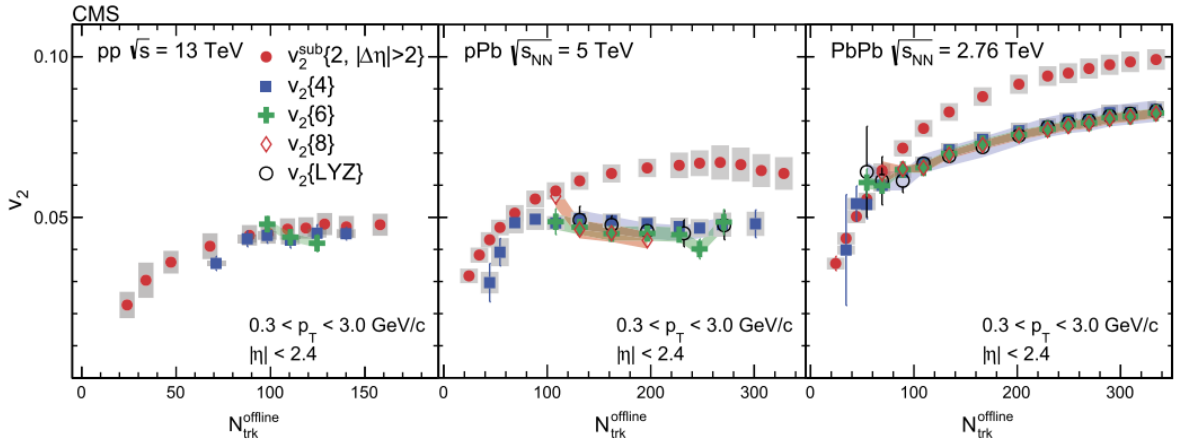

Figure 1.9: Elliptic flow measurements made using the 2nd, 4th, 6th, and 8th multi-particle cumulants, where the 2nd multi-particle is subtracted by peripheral events. Also the Lee Yang zero method non-flow elimination method is shown. These quantities are plotted vs the event multiplicity measured as $N_{trk}^{offline}$, which is the number of charged particle tracks observed during the offline analysis averaged over $0.3 < p_T < 3.0$ GeV/c and over $|\eta| < 2.4$. The left panel is $v_2^{sub}\{2, |\Delta\eta| > 2\}$, $v_2\{4\}$, and $v_2\{6\}$ in $p+p$ collisions at $\sqrt{s} = 13$ TeV. The middle panel $v_2^{sub}\{2, |\Delta\eta| > 2\}$, $v_2\{4\}$, $v_2\{6\}$, $v_2\{8\}$, and $v_2\{LYZ\}$ in $p+Pb$ at $\sqrt{s_{NN}}$= 5 TeV collisions. The right panel is $v_2^{sub}\{2, |\Delta\eta| > 2\}$, $v_2\{4\}$, $v_2\{6\}$, $v_2\{8\}$, and $v_2\{LYZ\}$ in $Pb+Pb$ collisions at $\sqrt{s_{NN}}$= 2.76 TeV. The error bars correspond to the statistical uncertainties, while the shaded regions correspond to the systematic uncertainties [18].

removing all lower-order correlations. This excellent agreement indicates that $p+Pb$ is similar to $Pb+Pb$ in that it is a N-body correlation, not a two-body decay or back-to-back jets which produces correlations between particles. Although these types of processes are present, all particles feel the effects of the initial geometry.

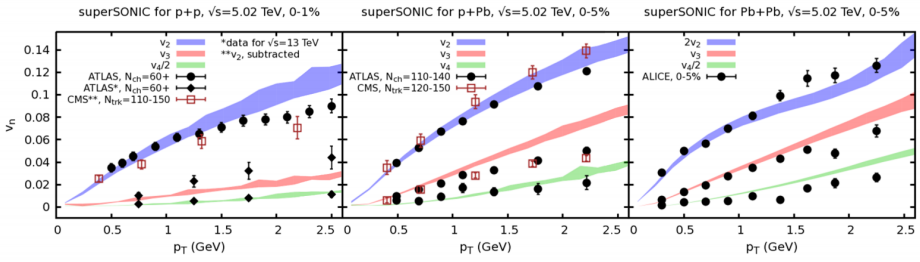

Figure 1.10: $v_2(p_T)$ for $d+Au$ and ^{3}He+Au at $\sqrt{s_{NN}}$= 200 GeV 0-5% centrality events for $\pi^{\pm}$ and $p+pbar$ separately. The boxes correspond to the systematic uncertainty. **add ref**

1.3.4 Measurements Made at RHIC

Flow measurements in small systems have also be made at a lower energy accelerator, RHIC. Small collision systems, $d+Au$, ^{3}He+Au, and $p+Au$ at $\sqrt{s_{_{NN}}}$= 200 GeV per nucleon were taken at RHIC in 2008, 2014, and 2015, respectively. The 2008 $d+Au$ dataset was intended to measure cold nuclear matter effects; however, RHIC experiments such as PHENIX had the capability to go back and measure $v_2(p_T)$. PHENIX was able to measure v_2 for $d+Au$ and for ^{3}He+Au for the 0-5% most central events, as shown in Figure 1.11. A substantial v_2 is observed for both $d+Au$ and ^{3}He+Au events with a p_T dependence, which is similar to that seen in $p+Pb$ at the LHC. Instead of subtracting the non-flow component, as was done in Figure 1.7, the non-flow is incorporated as a systematic uncertainty. In addition to the v_2 measurement, a substantial v_3 is measured for the ^{3}He+Au dataset. This measurement is significant because the observation of more than one flow indicates the system is exhibiting complex behavior. A single flow harmonic could be explained by a variety of causes, whereas two flow harmonics from the same system narrow the range of possible explanations.

In addition to measuring the $v_2(p_T)$ for all hadrons, v_2 has been measured for $\pi^{\pm}$ and p+$pbar$, as seen in Figure 1.12. A very similar mass ordering in $v_2(p_T)$ for different hadrons that was observed for $p+Pb$ at $\sqrt{s_{_{NN}}}$= 5.02 TeV in Figure 1.8, was also observed for $d+Au$ and ^{3}He+Au at $\sqrt{s_{_{NN}}}$= 200 GeV. In the low p_T region, $p_T < 1.5$ GeV, the v_2 for $\pi^{\pm}$ is greater than the v_2 for $p+pbar$. An interesting note here is that the low p_T region only goes up to 1.5 GeV/c, whereas the $p+Pb$ dataset shows a low p_T mass ordering region of up to 2 GeV/c. The reason for this is probably due to the difference in center of mass energy.

It is necessary to note that throughout all of these measurements in small systems, a skepticism to the interpretation that the measurements are hydrodynamic flow has persisted. There are alternative explanations to the apparent flow measured in small systems which do not involve the creation of a medium. In order to further the discussion on the distinction between a medium and a non-medium explanation, three different small collision systems, each with unique initial

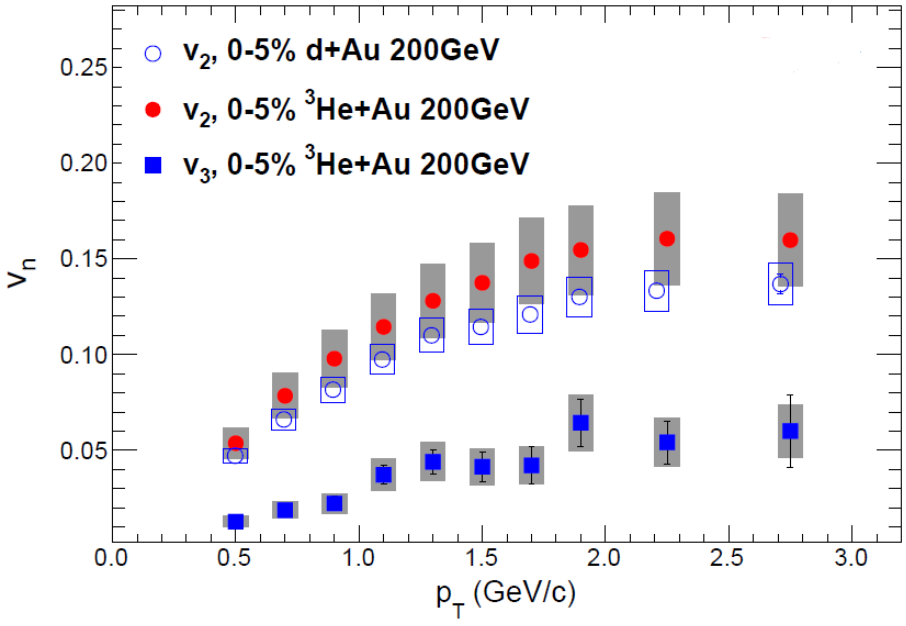

Figure 1.11: $v_n(p_T)$ measured for $d+Au$ and ^{3}He+Au at $\sqrt{s_{NN}}$= 200 GeV for 0-5% central events. v_2 was measured for both systems and v_3 was measured for ^{3}He+Au. The grey boxes correspond to systematic uncertainties. **add ref**

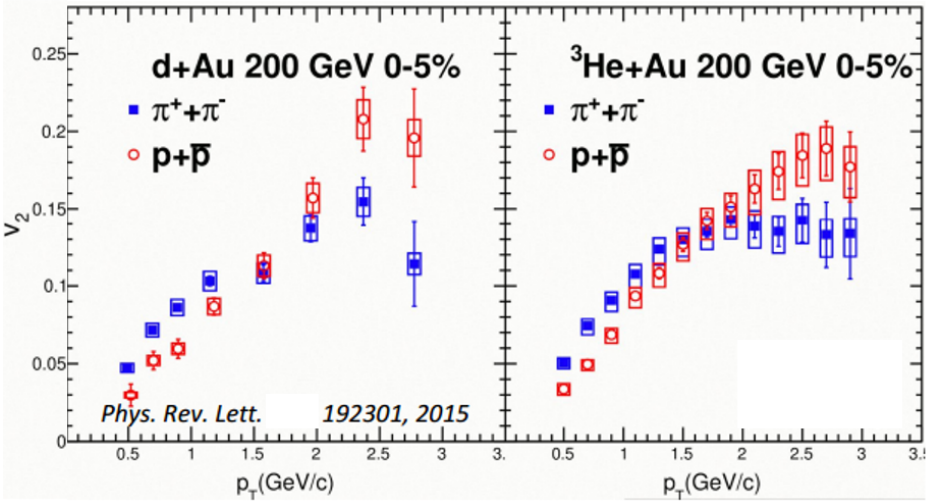

Figure 1.12: $v_2(p_T)$ for $d+Au$ and ^{3}He+Au at $\sqrt{s_{NN}}$= 200 GeV 0-5% centrality events for $\pi^{\pm}$ and $p+pbar$ separately. The boxes correspond to the systematic uncertainty. **add ref**

conditions, were run at RHIC. Those three systems are d+Au, He+Au, and finally p+Au, with intrinsic elliptical, triangular, and circular geometric initial conditions. The constraints that a set

of measurements from all three systems would place upon explanatory models would help distinguish which theory best describes small systems. This thesis is the completion of that set of three measurements, by measuring v_2 in the p+Au dataset.

Bibliography

[1]

[2] Event reconstruction in the {PHENIX} central arm spectrometers. Nucl.Instrum.Meth, A482:491–512, 2002.

[3] Rhic operations with asymmetric collisions in 2015. 2015.

[4] A. et al Adare. Measurements of elliptic and triangular flow in high-multiplicity ^{3}He + Au collisions at $\sqrt{s_{NN}} = 200$ GeV. Phys. Rev. Lett., 115:142301, Sep 2015.

[5] S. S. et al Adler. Absence of suppression in particle production at large transverse momentum in $\sqrt{s_{NN}} = 200$ GeV d + Au collisions. Phys. Rev. Lett., 91:072303, Aug 2003.

[6] J. et al Beringer. Review of particle physics. Phys. Rev. D, 86:010001, Jul 2012.

[7] Siegfried Bethke. The 2009 world average of α. The European Physical Journal C, 64(4):689–703, 2009.

[8] Fred Cooper and Graham Frye. Single-particle distribution in the hydrodynamic and statistical thermodynamic models of multiparticle production. Phys. Rev. D, 10:186–189, Jul 1974.

[9] S. Eremin and S. Voloshin. Nucleon participants or quark participants? Phys. Rev. C, 67:064905, Jun 2003.

[10] C. Aidala et al. The {PHENIX} forward silicon vertex detector. Nuclear Instruments and Methods in Physics Research Section A: Accelerators, Spectrometers, Detectors and Associated Equipment, 755:44 – 61, 2014.

[11] K. Adcox et al. {PHENIX} detector overview. Nuclear Instruments and Methods in Physics Research Section A: Accelerators, Spectrometers, Detectors and Associated Equipment, 499(2?3):469 – 479, 2003. The Relativistic Heavy Ion Collider Project: {RHIC} and its Detectors.

[12] A Fedotov. Progress of high-energy electron cooling for rhic.

[13] Enrico Fermi. High energy nuclear events. Progress of Theoretical Physics, 5(4):570–583, 1950.

[14] Charles Gale, Sangyong Jeon, Björn Schenke, Prithwish Tribedy, and Raju Venugopalan. Event-by-event anisotropic flow in heavy-ion collisions from combined yang-mills and viscous fluid dynamics. Phys. Rev. Lett., 110:012302, Jan 2013.

[15] M. Habich, J. L. Nagle, and P. Romatschke. Particle spectra and hbt radii for simulated central nuclear collisions of journal=.

[16] M. Habich, J. L. Nagle, and P. Romatschke. Particle spectra and hbt radii for simulated central nuclear collisions of c+c, al+al, cu+cu, au+au, and pb+pb from sqrt(s)=62.4-2760 gev. The European Physical Journal C, 75(1):15, 2015.

[17] Tetsufumi Hirano, Ulrich Heinz, Dmitri Kharzeev, Roy Lacey, and Yasushi Nara. Mass ordering of differential elliptic flow and its violation for ϕ mesons. Phys. Rev. C, 77:044909, Apr 2008.

[18] V. Khachatryan and et al. Evidence for collectivity in pp collisions at the {LHC}. Physics Letters B, 765:193 – 220, 2017.

[19] V. Khachatryan and etal. Observation of long-range, near-side angular correlations in proton-proton collisions at the lhc. Journal of High Energy Physics, 2010(9):91, 2010.

[20] Zi-Wei Lin, Che Ming Ko, Bao-An Li, Bin Zhang, and Subrata Pal. Multiphase transport model for relativistic heavy ion collisions. Phys. Rev. C, 72:064901, Dec 2005.

[21] Guo-Liang Ma and Zi-Wei Lin. Predictions for $\sqrt{s_{NN}} = 5.02$ tev pb + pb collisions from a multiphase transport model. Phys. Rev. C, 93:054911, May 2016.

[22] J. L. Nagle, A. Adare, S. Beckman, T. Koblesky, J. Orjuela Koop, D. McGlinchey, P. Romatschke, J. Carlson, J. E. Lynn, and M. McCumber. Exploiting intrinsic triangular geometry in relativistic ^{3}He + Au collisions to disentangle medium properties. Phys. Rev. Lett., 113:112301, Sep 2014.

[23] J. D. Orjuela Koop, A. Adare, D. McGlinchey, and J. L. Nagle. Azimuthal anisotropy relative to the participant plane from a multiphase transport model in central $p + \mathrm{Au}$, $d + \mathrm{Au}$, and ^{3}He + Au collisions at $\sqrt{s_{NN}} = 200$ gev. Phys. Rev. C, 92:054903, Nov 2015.

[24] A. M. Poskanzer and S. A. Voloshin. Methods for analyzing anisotropic flow in relativistic nuclear collisions. Phys. Rev. C, 58:1671–1678, Sep 1998.

[25] Johann Rafelski. Connecting qgp-heavy ion physics to the early universe. Nuclear Physics B - Proceedings Supplements, 243:155 – 162, 2013.

[26] P. Romatschke. Light-heavy-ion collisions: a window into pre-equilibrium qcd dynamics? The European Physical Journal C, 75(7):305, 2015.

[27] T. Roser. Rhic performance. Nuclear Physics A, 698(1):23 – 28, 2002.

[28] Bjrn Schenke and Raju Venugopalan. Collective effects in lightheavy ion collisions. Nuclear Physics A, 931:1039 – 1044, 2014. {QUARK} {MATTER} 2014XXIV {INTERNATIONAL} {CONFERENCE} {ON} {ULTRARELATIVISTIC} NUCLEUS-NUCLEUS {COLLISIONS}.

[29] Sren Schlichting and Bjrn Schenke. The shape of the proton at high energies. Physics Letters B, 739:313 – 319, 2014.

[30] Wilke van der Schee, Paul Romatschke, and Scott Pratt. Fully dynamical simulation of central nuclear collisions. Phys. Rev. Lett., 111:222302, Nov 2013.

[31] Kevin Welsh, Jordan Singer, and Ulrich Heinz. Initial-state fluctuations in collisions between light and heavy ions. Phys. Rev. C, 94:024919, Aug 2016.

[32] XIAO-MING XU. ORIGIN OF TEMPERATURE OF QUARK-GLUON PLASMA IN HEAVY ION COLLISIONS, pages 203–208. WORLD SCIENTIFIC, 2015.